Computational Science Laboratory Report CSL-TR-23-1 May 18, 2023

Ekansh Chaturvedi, Corina Sandu, Adrian Sandu

"Parametric formulations of spatial joints with clearances: A non-smooth dynamics approach"

Computational Science Laboratory
"Compute the Future!"

Department of Computer Science
Virginia Tech
Blacksburg, VA 24060
Phone: (540) 231-2193
Fax: (540) 231-6075
Email: ekanshchat96@vt.edu, csandu@vt.edu, sandu@cs.vt.edu
Web: https://csl.cs.vt.edu

Parametric formulations of spatial joints with clearances: A non-smooth dynamics approach

Ekansh Chaturvedi[1*], Corina Sandu[2†] and Adrian Sandu[3†]

[1*]Department of Mechanical Engineering, Virginia Tech, Blacksburg, 24060, Virginia, USA.
[2]Department of Mechanical Engineering, Virginia Tech, Blacksburg, 24060, Virginia, USA.
[3]Department of Computer Science, Virginia Tech, Blacksburg, 24060, Virginia, USA.

*Corresponding author(s). E-mail(s): ekanshchat96@vt.edu;
Contributing authors: csandu@vt.edu; sandu@cs.vt.edu;
†These authors contributed equally to this work.

Abstract

The conventional approach of simulating multibody dynamic systems treats the joint interfaces as ideal, that means that the bodies are in absolute alignment with each other in the desired relative directions of motion. However, in real life systems the clearances between the bodies allow the bodies to undergo a certain misalignment and the dynamics is governed by the contacts thus formed. Contact detection and evaluation of contact forces is yet another problem that needs to be addressed. Popular approaches assume the Hertzian nature of the contact and thus evaluate contact forces using nonlinear unilateral spring-damper elements. This approach results in very stiff differential algebraic equations and hence make the numerical integration computationally expensive. Furthermore, the Hertzian approach does not address truly elastic or truly inelastic nature of the contact. This work describes the parametric formulations for fundamental spatial joints with clearances and the non-smooth dynamics approach to solve the resulting equations of motion. The sets of spatial joint expressions for cylindrical, prismatic and revolute joints, and the non-smooth dynamics formulations are derived, considering their interdependence with great care. Further, the nature of the contact with clearances is discussed. The formulation is demonstrated through three case-studies and a detailed analysis of the results is presented. Additionally, a differentiation with respect to the ideal joint counterpart of the

revolute joint case study is presented using tangent space ordinary differential equation formulation.

Keywords: Non-smooth dynamics, Nonlinear dynamics, Joints with clearances, Contact dynamics, Constraints

1 Introduction

Modern methods for simulating multibody dynamics include algebraic constraint equations to represent mechanical joints. Such equations enforce absolute alignment of the connected bodies in the desired direction of relative motion, and thus represent "ideal joints". However, real mechanical systems have joints with clearances and the condition of absolute alignment is not always followed. In real-world applications, the motion is governed by intermittent formation of one or multiple contacts. The resulting contact forces are highly nonlinear phenomena that are challenging to model.

Corral et. al. [1] introduced a geometry-based contact model that considers penetration for evaluating displacement and restitution. One interesting feature of this model is that it formulates infinite planes to identify the contact points, however, this model does not combine well with differential algebraic equations (DAEs) or ordinary differential equations (ODEs) for constrained multibody systems.

Dopico et. al [2, 3] and Choi et. al [4] proposed a contact model that can be incorporated in index-3 DAE models. This approach uses a discretized mesh representation of geometry to identify the contact points. Therefore, the resulting constraint manifold is defined with equations corresponding to each node. These methods account for contact dynamics by forcing penalty factors using an augmented Lagrangian method. The equations of motion at the contact point are solved by projection of velocity and acceleration at contact points to solve for static equilibrium.

The contact model developed by Nikravesh and Lankarani [5] has been widely adopted, including in commercial software packages. This model uses a combination of nonlinear spring and damping elements to simulate the unilateral contact. Using this model, Shen et. al. [6] developed a formulation for simulating impact dynamics by using dynamic optimization with energy loss being the objective function. A drawback of this contact model is that high stiffness values of the nonlinear springs result in "stiff" differential equations, which require very small time-step sizes for numerical integration. Furthermore, separate detection of each contact and subsequent evaluation of contact forces, makes the approach computationally inefficient, especially when multiple contacts occur intermittently. Using interpenetration for evaluating contact forces violates the constraints manifold. Moreover, this approach does not address the correct nature of contact as elastic, semi-elastic, or inelastic and the resulting non-smooth nature of dynamic behavior in agreement with Newton's law of momentum conservation.

The popular approaches for modeling mechanical joints and the contact models discussed hitherto are not well suited for modeling joints with clearances. Dynamics with clearance in joints was studied in Sharf and Zhang [7] and [8]. Sharf and

Zhang in [7] founded the geometry-based contact models. Zakhariev [8] described an approach for calculating the reaction and friction forces between pairs of bodies in spatial mechanical systems, as well as contact points in joints with clearances. Matrix methods were used to derive the nonlinear kinematic constraint equations, and the external and inertia forces for each configuration of the kinematic chain the contact points and corresponding normal forces are calculated. A drawback of the methodology in [8] is that the derived equality constraints do not account for all the possible orientations of the contact formation.

Further developments regarding joints with clearance include the work by Ibrahimi et. al [9], Flores and Lankarani [10], and Xiang et. al [11], demonstrated through a number of simulations on planar systems formulated as DAEs and contact model referenced from [5]. Time independent sensitivity analysis for planar systems was also included in [9]. Bauchau et. al [12] used unilateral contact conditions to simulate planar and spatial joints by adding additional rotational state variables and using non-holonomic inequality constraints with introduction of slack variables.

Recently, the effectiveness of non-smooth dynamics approaches has been demonstrated in many-body dynamics problems such as simulation of sand particles, stacking of bricks, and stacking of multiple balls in a box [13–15]; in all these applications the formulation of constraints is straightforward. When implementing a non-smooth dynamics approach to multibody systems, a crucial aspect is be the formulation of constraints. Because of shape and geometry of the components, the constraint formulation should capture the possibilities of multiple contact points at different locations while retaining the analytical nature of the constraint expression. This requirement is necessary to build computationally efficient codes – in contrast to contact detection algorithms that use finite element discretization schemes of the solid bodies. Negrut et. al [16] described a methodology through which this can be achieved. The methodology poses the dynamics of the rigid bodies as a nonlinear programming problem (NLP) and uses dynamic optimization for minimizing an objective function derived from augmented Lagrangian approach.

This paper proposes an all-inclusive formulation for multibody system dynamics that can be used to simulate free bodies, systems with ideal constraints, systems having constraints with clearances, as well as impact dynamics. The contributions of this paper are as follows:

1. A general NLP formulation to discretize multibody dynamics is derived that encompasses equality as well as inequality constraints.
2. Analytical constraint expressions are derived for fundamental joints with clearances, which can be directly used in the NLP formulation.
3. The simulation methodology is applied to the case-studies of three fundamental mechanical joints with clearances: cylindrical, revolute and prismatic joints.

The remainder of this paper is structured as follows. Section 2 describes the general NLP formulation for time discretization of multibody systems. Section 3 formulates constraint expressions for spatial joints with clearances as functions of the rigid body pair's geometric features. Section 4 presents the case studies considered for testing the proposed formulation. Section 5 presents numerical results and discusses their

implications and section 6 concludes with key observations and a discussion on further scope of the work.

2 Methodology

2.1 Multibody dynamics in NLP formulation

This section illustrates the formulation of multibody systems in the general form of a nonlinear programming problem. The subsection 2.1.1 describes the equations of motion for rigid bodies undergoing motion in the absence of any constraints. The subsection 2.1.2 illustrates a method to evaluate contact forces on a set of rigid bodies. The subsection 2.1.3 combines the elements of free body dynamics and contact forces into an NLP of a general form. Finally, in the subsection 2.1.4, strategies to solve the general NLP problem through temporal discretization are discussed.

2.1.1 The free body dynamics

Formulation of equations of motion for three-dimensional systems in the body-frame coordinates results in a constant full rank and invertible 6×6 mass matrix for each body [17–19]. Considering these essential requirements, this section describes the free body dynamics.

Consider a rigid body of mass m, inertia matrix $\mathbf{J}$, generalized coordinates (placed at the center of mass) $\mathbf{q} = [\mathbf{r}^T, \mathbf{p}^T]^T \in \mathbb{R}^7$ in global frame, and the corresponding time derivatives of generalized coordinates $\dot{\mathbf{q}} = [\dot{\mathbf{r}}^T, \dot{\mathbf{p}}^T]^T \in \mathbb{R}^7$, where $\mathbf{r} \in \mathbb{R}^3$ is the set of Cartesian $[x, y, z]$ coordinates and $\mathbf{p} \in \mathbb{R}^4$ is the set of Euler parameters $[e_0, \mathbf{e}^T]^T$, all in global frame of reference. The equations of motion from D'Alembert's principle [20] are as follows:

$$\delta\mathbf{r}^T \left(m\,\ddot{\mathbf{r}} - \mathbf{F_A}\right) + \delta\boldsymbol{\pi}'^T \left(\mathbf{J}\,\dot{\boldsymbol{\omega}}' + \tilde{\boldsymbol{\omega}}'\,\mathbf{J}\,\boldsymbol{\omega}' - \mathbf{n}'_\mathbf{A}\right) = 0, \tag{1}$$

where $\delta\mathbf{r} \in \mathbb{R}^3$ are the infinitesimally small virtual displacements in global coordinate system and $\delta\boldsymbol{\pi}' \in \mathbb{R}^3$ and virtual rotations in body-fixed coordinate system. The operator '$\tilde{.}$' gives out the skew-symmetric matrix of the body-fixed vector of angular velocity $\boldsymbol{\omega}'$. The vector $\mathbf{F_A} \in \mathbb{R}^3$ represents externally applied forces in global reference frame and $\mathbf{n}'_\mathbf{A} \in \mathbb{R}^3$ are the externally applied torques in body-fixed reference frames. Equation (1) can thus be decomposed into the following set of equations in mixed reference frame system:

$$m\,\ddot{\mathbf{r}} = \mathbf{F_A}, \tag{2a}$$

$$\mathbf{J}\,\dot{\boldsymbol{\omega}}' + \tilde{\boldsymbol{\omega}}'\,\mathbf{J}\,\boldsymbol{\omega}' = \mathbf{n}'_\mathbf{A}, \tag{2b}$$

Equation (2) can be written in matrix form as follows:

$$\begin{bmatrix} m\mathbf{I} & \mathbf{0} \\ \mathbf{0} & \mathbf{J} \end{bmatrix} \begin{bmatrix} \ddot{\mathbf{r}} \\ \dot{\boldsymbol{\omega}}' \end{bmatrix} + \begin{bmatrix} \mathbf{0} \\ \tilde{\boldsymbol{\omega}}'\,\mathbf{J}\,\boldsymbol{\omega}' \end{bmatrix} - \begin{bmatrix} \mathbf{F_A} \\ \mathbf{n}'_\mathbf{A} \end{bmatrix} = \mathbf{0}, \tag{3}$$

Similarly, for a system of N bodies, the equation (3) takes the form:

$$\begin{bmatrix} m_1\mathbf{I} & \mathbf{0} & \mathbf{0} & \mathbf{0} & \mathbf{0} & \dots & \mathbf{0} \\ \mathbf{0} & \mathbf{J}_1 & \mathbf{0} & \mathbf{0} & \mathbf{0} & \dots & \mathbf{0} \\ \mathbf{0} & \mathbf{0} & m_2\mathbf{I} & \mathbf{0} & \mathbf{0} & \dots & \mathbf{0} \\ \mathbf{0} & \mathbf{0} & \mathbf{0} & \mathbf{J}_2 & \mathbf{0} & \dots & \mathbf{0} \\ \vdots & \vdots & \vdots & \vdots & \ddots & \vdots & \vdots \\ \mathbf{0} & \mathbf{0} & \mathbf{0} & \mathbf{0} & \dots & m_N\mathbf{I} & \mathbf{0} \\ \mathbf{0} & \mathbf{0} & \mathbf{0} & \mathbf{0} & \dots & \mathbf{0} & \mathbf{J}_N \end{bmatrix} \begin{bmatrix} \ddot{\mathbf{r}}_1 \\ \dot{\boldsymbol{\omega}}'_1 \\ \ddot{\mathbf{r}}_2 \\ \dot{\boldsymbol{\omega}}'_2 \\ \vdots \\ \ddot{\mathbf{r}}_N \\ \dot{\boldsymbol{\omega}}'_N \end{bmatrix} + \begin{bmatrix} \mathbf{0}_1 \\ \tilde{\boldsymbol{\omega}}'_1 \mathbf{J}_1 \boldsymbol{\omega}'_1 \\ \mathbf{0}_2 \\ \tilde{\boldsymbol{\omega}}'_2 \mathbf{J}_2 \boldsymbol{\omega}'_2 \\ \vdots \\ \mathbf{0}_N \\ \tilde{\boldsymbol{\omega}}'_N \mathbf{J}_N \boldsymbol{\omega}'_N \end{bmatrix} - \begin{bmatrix} \mathbf{F}_{\mathbf{A}1} \\ \mathbf{n}'_{\mathbf{A}1} \\ \mathbf{F}_{\mathbf{A}2} \\ \mathbf{n}'_{\mathbf{A}2} \\ \vdots \\ \mathbf{F}_{\mathbf{A}N} \\ \mathbf{n}'_{\mathbf{A}N} \end{bmatrix} = \mathbf{0}, \tag{4}$$

which in matrix form reads:

$$\mathbf{M}\,\dot{\mathbf{v}} + \mathbf{S}\,(\dot{\mathbf{q}}) - \mathbf{Q}_{\mathbf{A}} = \mathbf{0}. \tag{5}$$

In (5) $\dot{\mathbf{v}} \in \mathbb{R}^{6N}$ is the vector of time derivatives of the body-fixed velocity vector $\mathbf{v} \in \mathbb{R}^{6N}$ for N bodies. The matrix $\mathbf{M} \in \mathbb{R}^{6N\times 6N}$ combined mass matrix of N bodies in global coordinate system. The vector $\mathbf{S}\,(\dot{\mathbf{q}}) \in \mathbb{R}^{6N}$ represents the Coriolis force and the vector $\mathbf{Q}_{\mathbf{A}} \in \mathbb{R}^{6N}$ represents external forces and torque acting on the body neglecting friction, all in body fixed coordinate system. The mapping between the body-fixed angular velocity vector $\boldsymbol{\omega}'$ and the time derivatives of Euler parameters $\dot{\mathbf{p}}$ is given using the orthogonal matrix $\mathbf{G}(\mathbf{p})$ as follows [20]:

$$\begin{aligned} \mathbf{G}\,(\mathbf{p}) &\coloneqq \left[-\mathbf{e}\ -\tilde{\mathbf{e}} + e_0\mathbf{I}\right], \\ \dot{\mathbf{p}} &= \tfrac{1}{2}\,\mathbf{G}^T\,(\mathbf{p})\,\boldsymbol{\omega}', \\ \boldsymbol{\omega}' &= 2\,\mathbf{G}\,(\mathbf{p})\,\dot{\mathbf{p}}. \end{aligned} \tag{6}$$

Unless the contact happens, the bodies move freely as an unconstrained system, and have the unconstrained accelerations :

$$\dot{\mathbf{v}}_{\text{uc}} = -\mathbf{M}^{-1}\left(\mathbf{S}\,(\dot{\mathbf{q}}) - \mathbf{Q}_{\mathbf{A}}\right). \tag{7}$$

2.1.2 Dynamics with contact

Consider two bodies A and B in contact, as shown in Figure 1. Their respective centers of mass are c_A and c_B, and their coordinates in the global coordinate system are $\mathbf{r}_A$ and $\mathbf{r}_B$, respectively. The contact point is detected at a location indicated by body fixed vectors $\mathbf{s}'_A$ and $\mathbf{s}'_B$ in bodies A and B respectively. Let $\mathbf{n}_j$ be the normal unit vector along which the contact force acts on body A at the j^{th} contact, in global reference frame. This is required because all the forces are evaluated in global reference frame. The corresponding unit vector for body B will be $-\mathbf{n}_j$. If the magnitude of the contact force at the j^{th} contact is denoted by λ_j, the combined vector of the contact forces in global reference frame and the torques generated by them in body-fixed frame, can

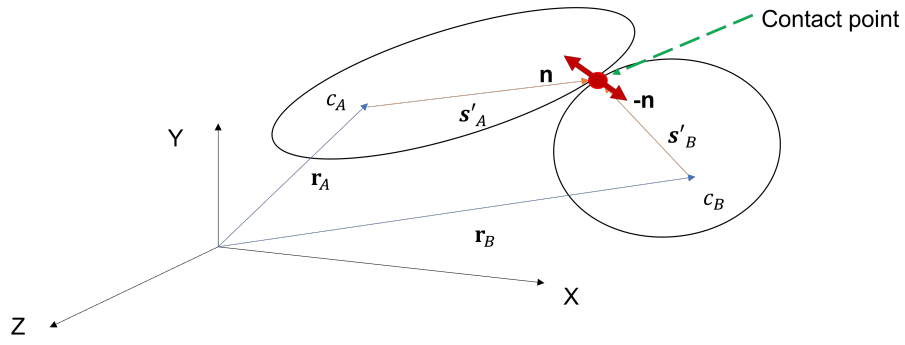

Fig. 1 Schematic representation of bodies in contact

be evaluated as follows [16]:

$$\mathbf{F_C}_j = \begin{bmatrix} \mathbf{n}_j \\ \tilde{\mathbf{s}}'_A \, \mathbf{A}^T(\mathbf{p}_A) \, \mathbf{n}_j \\ -\mathbf{n}_j \\ -\tilde{\mathbf{s}}'_B \, \mathbf{A}^T(\mathbf{p}_B) \, \mathbf{n}_j \end{bmatrix} \lambda_j = \mathbf{D}_j \, \lambda_j, \tag{8}$$

where $\mathbf{A} \in \mathbb{R}^{3\times3}$ is the rotation matrix as a function of the Euler parameters of bodies A and B, $\mathbf{D}_j \in \mathbb{R}^{6N\times1}$ is the contact matrix, and the operator '$\tilde{\cdot}$' gives out the skew-symmetric matrix of the underlying arbitrary vector. Similarly, for a number of possible M contacts between the two bodies, the total contact force $\mathbf{F_C}$ is the sum of all the contact forces acting on the respective bodies, where $\mathbf{D} \in \mathbb{R}^{6N\times M}$ and $\boldsymbol{\lambda} \in \mathbb{R}^{M\times1}$, is given as follows:

$$\mathbf{F_C} = \begin{bmatrix} \mathbf{D}_1 & \mathbf{D}_2 & \dots & \mathbf{D}_M \end{bmatrix} \begin{bmatrix} \lambda_1 \\ \lambda_2 \\ \vdots \\ \lambda_M \end{bmatrix} = \mathbf{D} \, \boldsymbol{\lambda}. \tag{9}$$

Using the same construct, the relative normal velocity between the two bodies at the contact point j in the mixed frame of reference is [16]:

$$\mathbf{v_{rel}}_j = \mathbf{D}_j^T \begin{bmatrix} \dot{\mathbf{r}}_A \\ \boldsymbol{\omega}'_A \\ \dot{\mathbf{r}}_B \\ \boldsymbol{\omega}'_B \end{bmatrix} = \mathbf{D}_j^T \, \mathbf{v}. \tag{10}$$

2.1.3 The nonlinear programming problem

Equation (7) is an expression to evaluate the unconstrained accelerations. The orthogonality of Euler parameters has to be enforced for each body as a bilateral equality

constraint [20]:

$$\mathbf{B}(\mathbf{q}) = \begin{bmatrix} \mathbf{p}_1^T\,\mathbf{p}_1 - 1 \\ \mathbf{p}_2^T\,\mathbf{p}_2 - 1 \\ \vdots \\ \mathbf{p}_N^T\,\mathbf{p}_N - 1 \end{bmatrix} = \mathbf{0}. \tag{11}$$

Therefore, there exists a set of Lagrange multipliers $\boldsymbol{\nu} \in \mathbb{R}^{N\times 1}$ such that:

$$\mathbf{M}\,\dot{\mathbf{v}} + \mathbf{B}_{\mathbf{q}}^T(\mathbf{q})\,\boldsymbol{\nu} + \mathbf{S}(\dot{\mathbf{q}}) - \mathbf{Q}_{\mathbf{A}} = \mathbf{0}, \tag{12}$$

where $\mathbf{B}_{\mathbf{q}}(\mathbf{q})$ is the Jacobian matrix of $\mathbf{B}(\mathbf{q})$ in equation (11).

Let the gap function $\boldsymbol{\Phi}^{\text{ineq}} \in \mathbb{R}^{M\times 1}$ represent the vector of algebraic inequalities for M unilateral contacts in the system. Let the condition of non-zero gap be be such that $\boldsymbol{\Phi}_j^{\text{ineq}} \leq \mathbf{0}$, $j \in 1, 2, \ldots, M$, where each element j of $\boldsymbol{\Phi}^{\text{ineq}}$ has a negative value. If the contact is formed, i.e., $\boldsymbol{\Phi}_j^{\text{ineq}} = \mathbf{0}$, $j \in 1, 2, \ldots, M$, the addition of the contact forces thus generated, $\mathbf{D}\,\boldsymbol{\lambda}$, results in constrained equation of motion as follows, where $\dot{\mathbf{v}}$ is the vector of constrained accelerations:

$$\dot{\mathbf{v}} = -\mathbf{M}^{-1}\left(\mathbf{S}\left(\dot{\mathbf{q}}\right) + \mathbf{B}_{\mathbf{q}}^T(\mathbf{q})\,\boldsymbol{\nu} + \mathbf{D}(\mathbf{q})\,\boldsymbol{\lambda} - \mathbf{Q}_{\mathbf{A}}\right), \tag{13a}$$

$$\boldsymbol{\Phi}^{\text{ineq}}\left(\mathbf{q}\right) * \boldsymbol{\lambda} = \mathbf{0}; \boldsymbol{\lambda} \geq \mathbf{0}, \tag{13b}$$

where the notation $\boldsymbol{\Phi}^{\text{ineq}}(\mathbf{q}) * \boldsymbol{\lambda}$ represents the element-wise product of every expression in the constraint manifold, and the corresponding magnitude of contact force. This complementarity condition states that when there is no contact, the j^{th} constraint expression $\boldsymbol{\Phi}_j^{\text{ineq}} < 0$, and the contact force's magnitude $\boldsymbol{\lambda}_j = 0$. However, when the contact happens, $\boldsymbol{\Phi}_j^{\text{ineq}} = 0$ and the contact force's magnitude $\boldsymbol{\lambda}_j > 0$.

Furthermore, Gauss' principle of least constraint [21] states that the true acceleration of a mechanical system of N masses $\ddot{\mathbf{r}}_j \in \mathbb{R}^3$, is the minimum of the following quantity:

$$\mathcal{J} = \sum_{j=1}^{N} m_j \left\| \ddot{\mathbf{r}}_j - \frac{\mathbf{F}_j}{m_j} \right\|^2 \quad \forall j \in [1, 2, 3, ..., N], \tag{14}$$

where the j^{th} particle has mass m_j, position vector $\mathbf{r}_j \in \mathbb{R}^3$, and applied vector of non-constraint force $\mathbf{F}_j \in \mathbb{R}^3$ acting on the mass. With a constant mass matrix $\mathbf{M}$ and plugging equations (7) and (13) in equation (14), the governing objective function for the system can be represented as the minimum of the difference in constrained and unconstrained accelerations as shown in equation (15).

$$\begin{aligned} \mathcal{J} &= \left(\dot{\mathbf{v}} - \dot{\mathbf{v}}_{\text{uc}}\right)^T \mathbf{M}\left(\dot{\mathbf{v}} - \dot{\mathbf{v}}_{\text{uc}}\right) \\ &= \left(\mathbf{M}^{-1}(\mathbf{D}\,\boldsymbol{\lambda} + \mathbf{B}_{\mathbf{q}}^T\,\boldsymbol{\nu})\right)^T \mathbf{M}\left(\mathbf{M}^{-1}(\mathbf{D}\,\boldsymbol{\lambda} + \mathbf{B}_{\mathbf{q}}^T\,\boldsymbol{\nu})\right). \end{aligned} \tag{15}$$

Since, $\mathbf{M}$ is a constant symmetric matrix, the equation (15) can be written as follows:

$$\mathcal{J} = \left(\mathbf{D}\,\boldsymbol{\lambda} + \mathbf{B}_{\mathbf{q}}^T\,\boldsymbol{\nu}\right)^T \mathbf{M}^{-1}\left(\mathbf{D}\,\boldsymbol{\lambda} + \mathbf{B}_{\mathbf{q}}^T\,\boldsymbol{\nu}\right). \tag{16}$$

Hence, the problem can be stated as a nonlinear programming problem (17) for the vector of state variables $\mathbf{Y} \coloneqq [\boldsymbol{\lambda}^T, \boldsymbol{\nu}^T, \dot{\mathbf{q}}^T, \mathbf{q}^T]^T$. Here the objective function (16) is minimized subject to the constraints imposed by equations of motion and the complementary constraints (13), and the normalized Euler parameters (11):

$$\begin{aligned} \hat{\mathbf{Y}} = \arg\min_{\mathbf{Y}} \quad & \left(\mathbf{D}\,\boldsymbol{\lambda} + \mathbf{B}_{\mathbf{q}}^T\,\boldsymbol{\nu}\right)^T \mathbf{M}^{-1} \left(\mathbf{D}\,\boldsymbol{\lambda} + \mathbf{B}_{\mathbf{q}}^T\,\boldsymbol{\nu}\right) \\ \text{s.t.} \quad & \mathbf{M}\,\dot{\mathbf{v}} + \mathbf{B}_{\mathbf{q}}^T(\mathbf{q})\,\boldsymbol{\nu} + \mathbf{D}(\mathbf{q})\,\boldsymbol{\lambda} + \mathbf{S}\left(\dot{\mathbf{q}}\right) - \mathbf{Q}_{\mathbf{A}} = \mathbf{0}, \\ & \mathbf{B}(\mathbf{q}) = 0, \\ & \boldsymbol{\Phi}^{\text{ineq}}\left(\mathbf{q}\right) \leq \mathbf{0} \perp \boldsymbol{\lambda} \geq \mathbf{0}. \end{aligned} \tag{17}$$

Furthermore, to simulate a multibody system with a combination of equality type constraints $\boldsymbol{\Phi}^{\text{eq}} = \mathbf{0}$, i.e., for ideal joints, the manifold $\boldsymbol{\Phi}^{\text{eq}}$ can be appended to the bilateral constraint manifold (11). However, this study focuses only on the system made of joints with clearances and therefore the ideal joint constraints are excluded from this study. Nevertheless, the capacity of the described NLP formulation to deal with ideal as well as contact-driven constraints makes it an all-inclusive formulation.

2.1.4 Discretization and solution strategy

Consider now the discrete version of the dynamics. At time t_{n-1} one has available the global frame time derivatives of generalized coordinates $\dot{\mathbf{q}}_{n-1}$, the velocities $\mathbf{v}_{n-1}$, and the positions of the generalized coordinates $\mathbf{q}_{n-1}$ as follows:

$$\mathbf{q}_{n-1} = \left[\mathbf{r}_{n-1}^T \;\; \mathbf{p}_{n-1}^T\right]^T, \tag{18a}$$

$$\mathbf{v}_{n-1} = \left[\dot{\mathbf{r}}_{n-1}^T \;\; \left(2\,\mathbf{G}\left(\mathbf{p}_{n-1}\right)\dot{\mathbf{p}}_{n-1}\right)^T\right]^T, \tag{18b}$$

$$\dot{\mathbf{q}}_{n-1} = \left[\dot{\mathbf{r}}_{n-1}^T \;\; \dot{\mathbf{p}}_{n-1}^T\right]^T. \tag{18c}$$

Let h_n be the time-step size. Then, at the new derivatives of generalized coordinates $\dot{\mathbf{q}}_n$, the velocities $\mathbf{v}_n$, and the positions of the generalized coordinates $\mathbf{q}_n$ must be evaluated, at time $t_n = t_{n-1} + h_n$. Hence, using half implicit Euler's expansion [22] we have the following relationships:

$$\dot{\mathbf{q}}_n = \left[\dot{\mathbf{r}}_n^T \;\; \dot{\mathbf{p}}_n^T\right]^T, \tag{19a}$$

$$\mathbf{q}_n = \mathbf{q}_{n-1} + h_n \dot{\mathbf{q}}_n \tag{19b}$$

$$\mathbf{v}_n = \left[\dot{\mathbf{r}}_n^T \;\; \left(2\,\mathbf{G}\left(\mathbf{p}_{n-1}\right)\dot{\mathbf{p}}_n\right)^T\right]^T, \tag{19c}$$

$$\dot{\mathbf{v}}_n = \frac{\mathbf{v}_n - \mathbf{v}_{n-1}}{h_n}, \tag{19d}$$

$$t_n = t_{n-1} + h_n. \tag{19e}$$

The bilateral constraint expressions (11) can be further discretized using Taylor's expansion. The unilateral constraints can be discretized using the relative velocities

in equation (10). These discretizations are represented in the following equations:

$$\mathbf{B}\left(\mathbf{q}_n\right) = \mathbf{B}\left(\mathbf{q}_{n-1}\right) + h_n\, \mathbf{B}_{\mathbf{q}}(\mathbf{q}_{n-1})\, \dot{\mathbf{q}}_n = \mathbf{0}, \tag{20}$$

$$\mathbf{\Phi}^{\text{ineq}}(\mathbf{q}_n) = \mathbf{\Phi}^{\text{ineq}}(\mathbf{q}_{n-1}) + h_n\, \mathbf{D}^T(\mathbf{q}_{n-1})\, \mathbf{v}_n \leq \mathbf{0}. \tag{21}$$

Incorporating equations (18), (19), (20) and (21) in NLP (17) we get the following NLP in discretized form, with respect to the vector of optimization variables $[h_n, \mathbf{Y}_n]$:

$$\begin{aligned} \left[\hat{h}_n, \hat{\mathbf{Y}}_n\right] = \arg\min_{h_n, \mathbf{Y}_n} \quad & \mathbf{T}_n^T\, \mathbf{M}^{-1}\, \mathbf{T}_n \\ \text{s.t.} \quad & \mathbf{M}(\mathbf{v}_n - \mathbf{v}_{n-1}) + h_n\, \mathbf{K}_n = \mathbf{0}, \\ & \mathbf{B}(\mathbf{q}_{n-1}) + h_n\, \mathbf{B}_{\mathbf{q}}(\mathbf{q}_{n-1})\, \dot{\mathbf{q}}_n = \mathbf{0}, \\ & \mathbf{\Phi}^{\text{ineq}}(\mathbf{q}_{n-1}) + h_n\, \mathbf{D}_{n-1}^T\, \mathbf{v}_n \leq \mathbf{0}, \\ & \boldsymbol{\lambda}_n \geq \mathbf{0}, \\ & h_{\max} \geq h_n \geq h_{\min}, \end{aligned} \tag{22}$$

where $\hat{h}_n$ and $\hat{\mathbf{Y}}_n$ are the resulting step size and solution, respectively, and $\mathbf{T}_n$ and $\mathbf{K}_n$ are defined as follows:

$$\mathbf{T}_n \coloneqq \mathbf{D}(\mathbf{q}_{n-1})\, \boldsymbol{\lambda}_n + \mathbf{B}_{\mathbf{q}}^T(\mathbf{q}_{n-1})\, \boldsymbol{\nu}_n, \tag{23a}$$

$$\mathbf{K}_n \coloneqq \mathbf{T}_n + \mathbf{S}\ (\dot{\mathbf{q}}_{n-1}) - \mathbf{Q}_{\mathbf{A}}(\mathbf{q}_{n-1}). \tag{23b}$$

Here, the optimal values of h_n, $\boldsymbol{\lambda}_n$, $\boldsymbol{\nu}_n$ and $\dot{\mathbf{q}}_n$ need to be found at time t_n. The scalar terms $h_{\min}$ and $h_{\max}$ respectively, are the minimum and maximum finite positive values of time-step size. Once the optimization problem (22) has been solved at a time t_n, the value of $\dot{\mathbf{q}}_n$ and h_n can then be utilized to evaluate and store the accelerations $\dot{\mathbf{v}}_n$ and the positions $\mathbf{q}_n$ using equations (19).

It must be mentioned here that the approach described in this section inherently assumes an inelastic nature of the contact, which is suitable for the scope of this work. The clearances are very small compared to the other dimensions of the components in a machine and hence the components do not gain enough pre-collision velocities for the contact to fall in the elastic domain.

2.2 Algorithm

A step-by-step procedure to implement the formulation discussed in the previous section has been explained in the algorithm 1. For a target simulation time $t_{\max}$, the initial values of $\mathbf{Y}_0$ at time t_0 should be such that all constraint equations are satisfied. For the initial values of generalized coordinates satisfying a negative value of gap function, the initial value of Lagrangian multipliers $\boldsymbol{\lambda}_0$ should be assumed zero.

Algorithm 1 Non-smooth multibody dynamics

1: **Inputs:** $t_0, t_{\text{final}}, h_{\min}, h_{\max}, \mathbf{Y}_0$ ▷ The initial states $\mathbf{Y}_0 = [\boldsymbol{\lambda}_0^T, \boldsymbol{\nu}_0^T, \dot{\mathbf{q}}_0^T]^T$
2: $n \leftarrow 0$
3: **while** $t_n < t_{\text{final}}$ **do**
4: $\quad n \leftarrow n + 1$
5: $\quad \begin{cases} \hat{h}_{\min} = \min\{h_{\min}, t_{\text{final}} - t_{n-1}\} \\ \hat{h}_{\max} = \min\{h_{\max}, t_{\text{final}} - t_{n-1}\} \end{cases}$ ▷ Ensure $t_n \leq t_{\text{final}}$
6: $\quad [h_n, \mathbf{Y}_n] \leftarrow$ Solution of NLP$(\mathbf{Y}_{n-1}, \hat{h}_{\min}, \hat{h}_{\max})$ ▷ Solve (22)
7: $\quad [\boldsymbol{\lambda}_n^T, \boldsymbol{\nu}_n^T, \dot{\mathbf{q}}_n^T] \coloneqq \mathbf{Y}_n^T$ ▷ Extract the state variables
8: $\quad \begin{bmatrix} \mathbf{q}_n \\ \mathbf{v}_n \\ \dot{\mathbf{v}}_n \end{bmatrix} \leftarrow \begin{bmatrix} \mathbf{q}_{n-1} + h_n \dot{\mathbf{q}}_n \\ \left[\dot{\mathbf{r}}_n^T \;\; (2\,\mathbf{G}\,(\mathbf{p}_{n-1})\,\dot{\mathbf{p}}_n)^T\right]^T \\ \frac{1}{h_n}(\mathbf{v}_n - \mathbf{v}_{n-1}) \end{bmatrix}$ ▷ from equation (19)
9: $\quad t_n \leftarrow t_{n-1} + h_n$
10: **end while**

The values of state variables obtained at the n^{th} time-step in step 7 of the algorithm 1, can be later used to evaluate contact forces and torques using the equation (9).

3 Formulation of constraints with clearances for specific joints

In this section, the formulations for three fundamental joints used in mechanical systems are presented. The gap function $\boldsymbol{\Phi}^{\text{ineq}}$ should provide both the normal distance and the normal unit vector between the potential contact points to suit the equation (8). Keeping this key requirement in consideration, the parametric formulations for joints with clearances are presented in this section.

3.1 Cylindrical joint with clearances

Figure 2 shows a system of two bodies i and j forming a cylindrical pair with radial clearance c. The generalized coordinates of bodies are $\mathbf{q}_i \in \mathbb{R}^7$ and $\mathbf{q}_j \in \mathbb{R}^7$ respectively. Let points P_{i_1} and P_{i_2} represent the two ends of center-line of body i in global frame of reference. Let points P_{j_1} and P_{j_1} represent the two ends of center-line of body j in global frame of reference. The perpendicular distances of points P_{i_1} and P_{i_2} from the center axis of body j are d_{s_1} and d_{s_2}, along the unit vectors $\mathbf{n}_{s_1}$ and $\mathbf{n}_{s_2}$ respectively. Let $\mathbf{A}(\mathbf{p}_i)$ and $\mathbf{A}(\mathbf{p}_j)$ be the rotation matrices of the respective bodies. Given the local coordinate vector $\mathbf{s}'_{k_x}$ of an arbitrary point P_{k_x} with $x \in [1, 2]$ in a body with respect to the centroid $k \in [i, j]$, the position of point P_{k_x} can be evaluated in global frame as $\mathbf{r}_{k_x}$ using equation (24).

$$\mathbf{r}_{k_x} = \mathbf{r}_k + \mathbf{A}(\mathbf{p}_k)\,\mathbf{s}'_{k_x}. \tag{24}$$

The body with the smaller axial length will have one or both of the end faces making

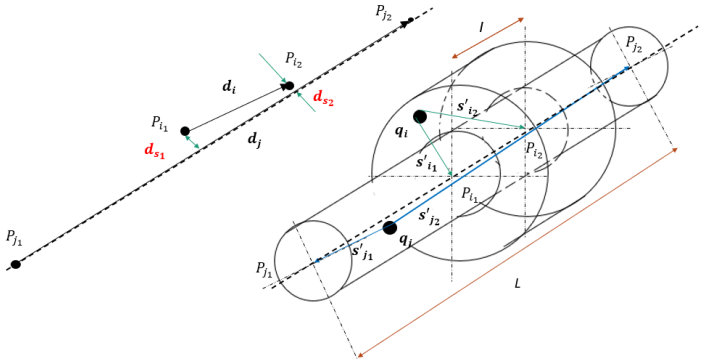

Fig. 2 Schematic representation of a spatial cylindrical joint with clearance

contact with the longer body. Assuming that body i it the smaller body and considering P_{j_1} as the reference point with position vector $\mathbf{r}_{j_1}$, the perpendicular vectors $\mathbf{d}_{s_x}$, $x \in [1, 2]$ pointing towards the contact points P_{k_x} can be evaluated via the following equations:

$$\mathbf{d}_{s_x} = (\mathbf{r}_{i_x} - \mathbf{r}_{j_1}) - (\mathbf{r}_{i_x} - \mathbf{r}_{j_1}) \frac{(\mathbf{r}_{i_x} - \mathbf{r}_{j_1})^T (\mathbf{r}_{j_2} - \mathbf{r}_{j_1})}{\|\mathbf{r}_{i_x} - \mathbf{r}_{j_1}\| \, \|\mathbf{r}_{j_2} - \mathbf{r}_{j_1}\|}, \tag{25}$$

$$\mathbf{n}_{s_x} = \frac{\mathbf{d}_{s_x}}{\|\mathbf{d}_{s_x}\|} = \frac{\mathbf{d}_{s_x}}{d_{s_x}}. \tag{26}$$

Considering c of a very small magnitude in comparison to other dimensions of the components, the perpendicular distances d_{s_1} and d_{s_2} must abide the following inequalities:

$$\mathbf{\Phi}^{\text{cylindric}}(\mathbf{q}) = \begin{bmatrix} d_{s_1} - c \\ d_{s_2} - c \end{bmatrix} \leq \mathbf{0}. \tag{27}$$

Assuming the hole inside the body i has a radius R, the position of the corresponding contact points $\mathbf{c}_x$ in the global reference frame can be calculated as:

$$\mathbf{c}_x = \mathbf{r}_i + \mathbf{A}(\mathbf{p}_i)(\mathbf{s}'_{i_x} - R\,\mathbf{n}_{s_x}). \tag{28}$$

3.2 Prismatic joint with clearances

Figure 3 shows a system of two bodies, i and j, forming a prismatic pair with clearance. The generalized coordinates of the bodies are $\mathbf{q}_i \in \mathbb{R}^7$ and $\mathbf{q}_j \in \mathbb{R}^7$ respectively. The prismatic joint with a clearance poses a special intricacy because of its exclusive dependence on geometric parameters. Traditionally, a prismatic joint consists of shapes with vertices and planes to constrain the rotational motion about the longitudinal axis and these vertices form the contact points. A prismatic joint without clearance does not require these to be included, as the contact forces are not evaluated on individual vertex. However, when clearance is included, each vertex of the inner body (minimum 6 are required for a spatial prismatic joint) needs to be individually constrained to not penetrate the enveloping body's two adjacent planes. Hence, the geometric locations

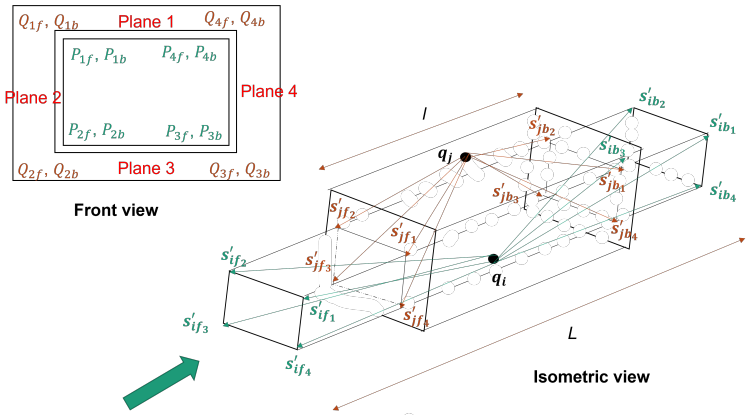

Fig. 3 Schematic representation of a spatial prismatic joint with clearance

of all the vertices are required with respect to the local coordinate system. As visible from the front view, each vertex of body i (inner body) at front and back faces, is constrained to two adjacent planes. For example, points P_{4f} and P_{4b} are constrained to planes 1 and 4, points P_{1f} and P_{1b} are constrained to plane 1 and plane 3, and so on. It requires at least three points to define a plane. The planes 1-4 are defined by the vertices in the above figure. For example, plane 1 is defined using points Q_{1f}, Q_{4f} and Q_{4b}, plane 2 is defined by P_{1f}, P_{2f}, P_{1b}, and so on.

With this methodology, a polygon of any regular or irregular shape can be defined with the help of all the vertices and planes. Each vertex of an N sided polygon is constrained to two adjacent planes at both the faces. This results in $4N$ equations of distance constraint. Obviously, each vertex's global coordinates need to be calculated as per equation (24). The perpendicular distance between a point P on body i, where $P \in [P_{1f}, P_{2f}, \ldots, P_{Nf}, P_{1b}, P_{2b}, \ldots, P_{Nb}]$, and a plane obtained from vertices on body j can be calculated as:

$$d_P = (\mathbf{r}_P - \mathbf{r}_Q)^T \mathbf{n}_{QP} \geq 0, \tag{29}$$

where, $\mathbf{n}_{QP}$ is the normal vector of the bounding plane pointing towards the point P, Q is any point in the bounding plane, and $\mathbf{r}_P$ and $\mathbf{r}_Q$ are the vectors associated with point P and point Q in global reference frame evaluated with equation (24). Hence, for a pair of rigid bodies forming a prismatic joint, with the internal body having $2M$ vertices and bounded by external body having M planes, the constraint manifold is

given as per the following inequality.

$$\mathbf{\Phi}^{\text{prismatic}}(\mathbf{q}) = \begin{bmatrix} -d_{P_{f1}} \\ \vdots \\ -d_{P_{f2M}} \\ -d_{P_{b1}} \\ \vdots \\ -d_{P_{b2M}} \end{bmatrix}_{4M\times 1} \leq \mathbf{0}. \tag{30}$$

Here, the subscripts 'f' and 'b' respectively signify the vertices in front and back, as shown in Figure 3.

3.3 Revolute joint with clearances

The spatial revolute joint is essentially an axially constrained cylindrical joint. Let body i in Figure 2 be axially constrained at the ends of body j such that there remains an axial clearance c_a. The normal vectors $\mathbf{n}_{j_1}$ and $\mathbf{n}_{j_2}$ at the constraining planes at P_{j_1} and P_{j_2}, respectively, are evaluated as per the following equations:

$$\mathbf{n}_{j_1} = \frac{\mathbf{r}_{j_2} - \mathbf{r}_{j_1}}{\|\mathbf{r}_{j_2} - \mathbf{r}_{j_1}\|}, \qquad \mathbf{n}_{j_2} = -\mathbf{n}_{j_1}. \tag{31}$$

Consequently, the construction of the joint requires that the distance of points P_{i_1} and P_{i_2} from P_{j_1} and P_{j_2}, projected on the normal vectors $\mathbf{n}_{j_1}$ and $\mathbf{n}_{j_2}$, respectively, is positive.

$$\begin{aligned} -(\mathbf{r}_{i_1} - \mathbf{r}_{j_1})^T \mathbf{n}_{j_1} \leq 0, \\ -(\mathbf{r}_{i_2} - \mathbf{r}_{j_2})^T \mathbf{n}_{j_2} \leq 0. \end{aligned} \tag{32}$$

Hence, the constraint manifold for a revolute joint with clearances is given as the following set of inequalities:

$$\mathbf{\Phi}^{\text{revolute}}(\mathbf{q}) = \begin{bmatrix} \mathbf{\Phi}^{\text{cyl}}(\mathbf{q}) \\ -(\mathbf{r}_{i_1} - \mathbf{r}_{j_1})^T \mathbf{n}_{j_1} \\ -(\mathbf{r}_{i_2} - \mathbf{r}_{j_2})^T \mathbf{n}_{j_2} \end{bmatrix} \leq \mathbf{0}. \tag{33}$$

4 Case studies

This section discusses the three relevant case studies that were used to test the methodology discussed in sections 2 and 3.

4.1 Case study: Cylindrical joint

Figure 4 shows a simple case study of a spatial cylindrical joint with clearance to illustrate the proof of concept for the proposed formulation. The case study comprises

of a slider of mass m with its center of mass denoted by the generalized coordinates $\mathbf{q} \in \mathbb{R}^7$ and a mass-less rod or radius R fixed at both ends. There is a radial clearance $c = 0.1mm$ between the slider and the rod and gravity acts along the $-\mathbf{Y}$ axis. An external force F acts on the slider at a point marked by a body-frame vector $\mathbf{s}'_f$. The system specific details illustrated in Figure 4 are shown in Table 1.

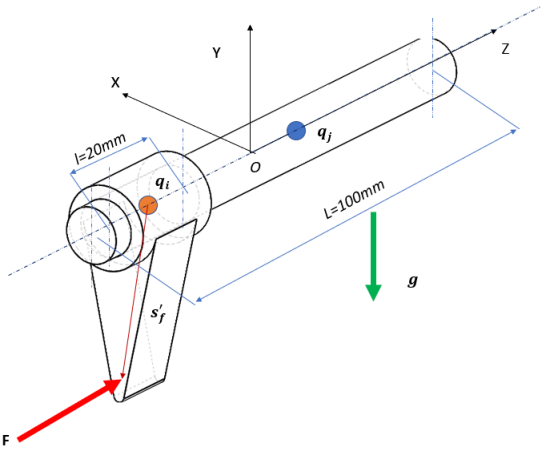

Fig. 4 Schematic diagram of the cylindrical pair with clearance

Table 1 Case study specifications: Cylindrical pair

Property	Value	Units
m	3.2	kg
L	100	mm
l	20	mm
R	5	mm
$\|\mathbf{s}'_f\|$	30	mm
F	50	N

4.2 Case study: Prismatic joint

Figure 5 shows a simple case study of a spatial prismatic joint with clearance $c = 0.3mm$. As it can be observed, the bodies have triangular cross-section with each edge of the cavity in body j of length e_j; the corresponding length for body i is e_i. The slider i has mass m with its center of mass denoted by the generalized coordinates $\mathbf{q} \in \mathbb{R}^7$ and a mass-less triangular prism is fixed at both ends. The gravity acts along the $-\mathbf{Y}$ axis and an external force F acts on the slider at a point marked by a body-frame vector $\mathbf{s}'_f$. The topmost vertices of the slider are labeled P_{f_1} and P_{b_1} respectively.

The trajectory of these two contact points is tracked and discussed in section 5.2. The system specific details illustrated in Figure 5 are shown in Table 2.

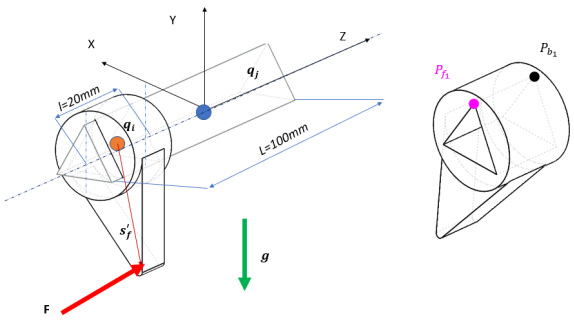

Fig. 5 Schematic diagram of the triangular prismatic pair with clearance

Table 2 Case study specifications.

Property	Value	Units
m	3.2	kg
L	100	mm
l	20	mm
e_i	17.67	mm
e_j	17.32	mm
$\|\mathbf{s}'_f\|$	30	mm
F	40	N

4.3 Case study: Revolute joint

Figure 6 shows a simple case study of a pendulum i forming a revolute joint with a hinge pin j of radius R. The radial and axial clearances are designated by c and c_a. The center of mass of the pendulum is located at cm_x and cm_x units along local X and Z directions. As can be observed, the bob of the pendulum is a rod protruding out of the XZ plane. This odd shape has been chosen to induce motion along Z direction as well. The pendulum i has mass m with its center of mass denoted by the generalized coordinates $\mathbf{q} \in \mathbb{R}^7$ and the hinge pin j is mass-less and fixed at both ends. The gravity acts along the $-\mathbf{Y}$ axis. The system specific details illustrated in Figure 6 are shown in Table 3.

5 Results and discussion

The simulation results were achieved using sequential quadratic programming (SQP). The case-studies of cylindrical and prismatic joints were conducted with time step

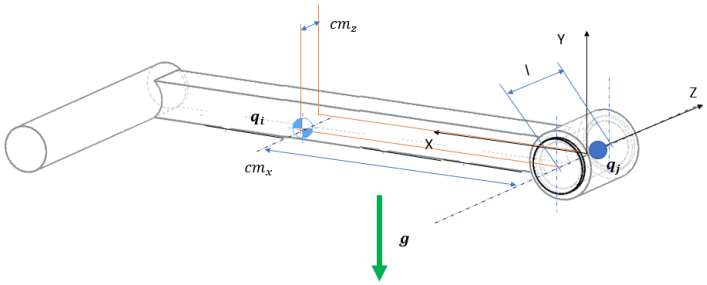

Fig. 6 Schematic diagram of the revolute pair with clearance

Table 3 Case study specifications: Revolute pair

Property	Value	Units
m	2	kg
l	20	m
c	0.1	m
R	5	m
c_a	0.1	m
cm_x	30.9	m
cm_z	11.97	m

h varying between $h_{\min} = 10^{-3}$ and $h_{\max} = 10^{-2}$ seconds while the revolute joint case study was conducted with h varying between $h_{\min} = 10^{-3}$ and $h_{\max} = 2 \times 10^{-3}$ seconds. The SQP algorithm comes with the advantage of fast convergence and its ability to efficiently deal with large number of constraints [23]. The constraint violation was observed $\|\mathbf{\Phi}^{\text{ineq}}(\mathbf{q})\| \leq 10^{-10}$ upon the contact formation. At the same time the equations of motion (13) were satisfied within the limits of 10^{-9}.

5.1 Cylindrical pair

Figure 7 shows the positions of X and Y components of the left hand and the right hand ends of the slider. As can be expected, the external force F generates a torques and tilts the slider. After the contact is formed at the diametrically opposite ends of the rod j, the slider starts moving in the Z direction. Figure 8 shows the contact forces $CF - x$, $CF - y$ and $CF - z$ in X, Y and Z directions respectively. Figure 9 represents the X and Y velocities of the center of mass and Figure 10 represents the Z-velocity of the center of mass. Figures 11 and 12 respectively represent the positions of center of mass in X-Y direction and Z direction and the Figure 13 shows the step-size adaptation over time. It can be observed that the dramatic fluctuations in the step-size correlate well with the lateral micro-oscillations of the contact points that undergo sliding while maintaining the contact, as observed in the 7.

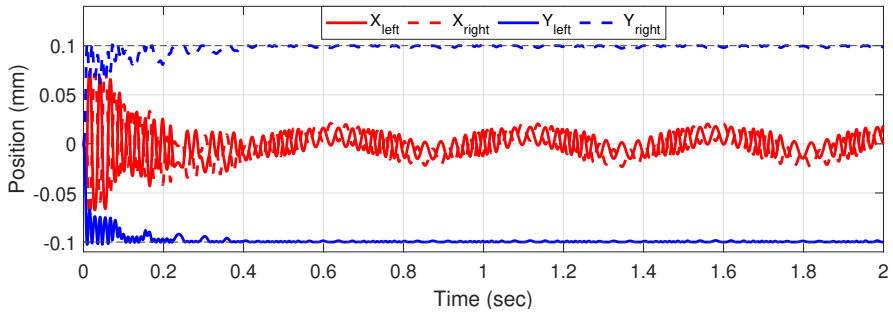

Fig. 7 Cylindrical pair: X and Y coordinates of the centers of left and right ends.

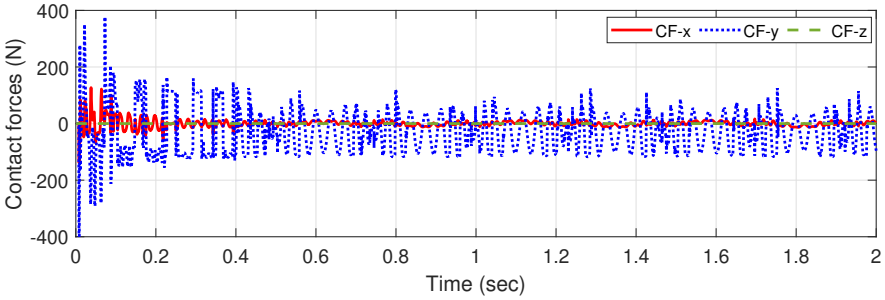

Fig. 8 Cylindrical pair: Contact forces against time.

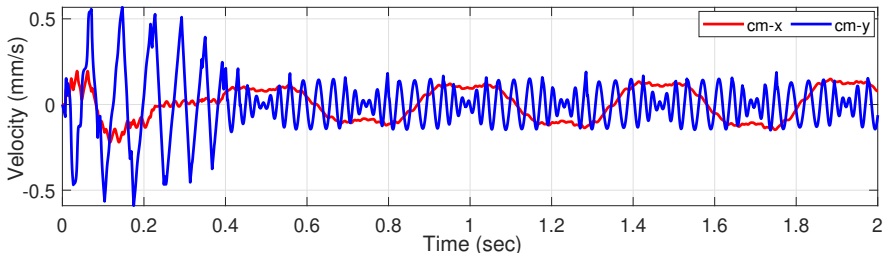

Fig. 9 Cylindrical pair: X and Y velocities of center of mass.

5.2 Prismatic pair

Figure 14 shows the positions of Y components of the points P_{f_1} and P_{b_1} shown in Figure 5. The external force F generates a torques and tilts the slider, similar to in cylindrical pair's case. However, the contact happens on all the 6 vertices. After the contact is formed at the of the body j, the slider starts moving in the Z direction. Figure 15 shows the contact forces $CF-x$, $CF-y$ and $CF-z$ in X, Y and Z directions respectively. Figure 16 represents the X and Y velocities of the center of mass and Figure 17 represents the Z-velocity of the center of mass. Figures 18 and 19 respectively represent the positions of center of mass in X-Y direction and Z direction. The Figure

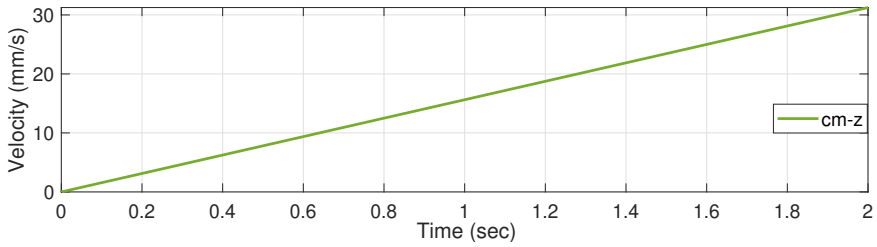

Fig. 10 Cylindrical pair: Z velocity of center of mass.

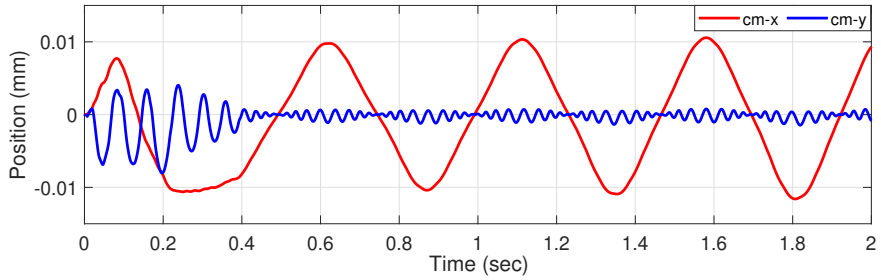

Fig. 11 Cylindrical pair: X and Y coordinates of center of mass.

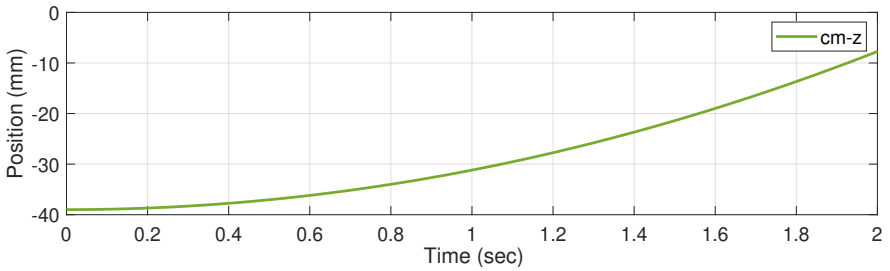

Fig. 12 Cylindrical pair: Z coordinate of center of mass.

5.2 represents the step-size adaptations against time. It can be observed that the once a steady contact is maintained, the step-size also stabilizes to the maximum value of 10^{-2}, while minute oscillations in the positions of the contact points in relative sliding, as observed in the case of cylindrical pair in 13, results in oscillatory behavior of the step-size.

5.3 Revolute pair

In this section, the results obtained from the proposed methodology have been discussed for the revolute pair case study. The counterparts from an ideal joint case, i.e., without any clearance have also been compared. The ideal joint case was evaluated

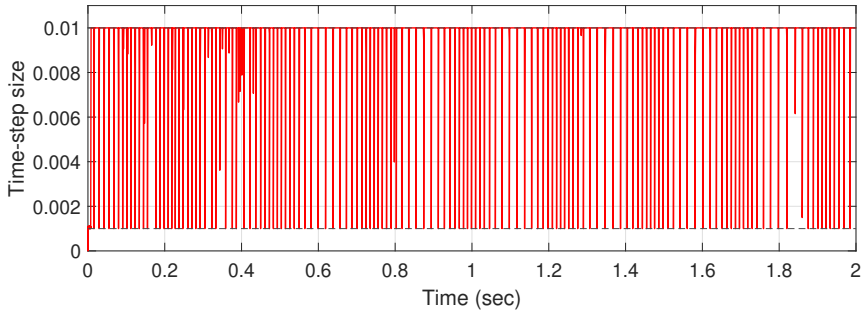

Fig. 13 Cylindrical pair: Time step size.

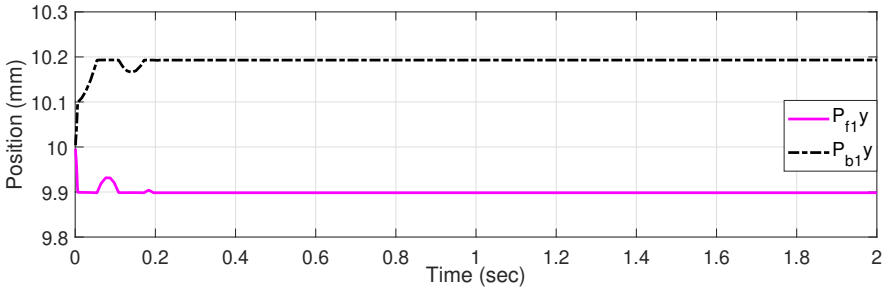

Fig. 14 Prismatic pair: Y coordinates of contact points P_{f1} and P_{f2}.

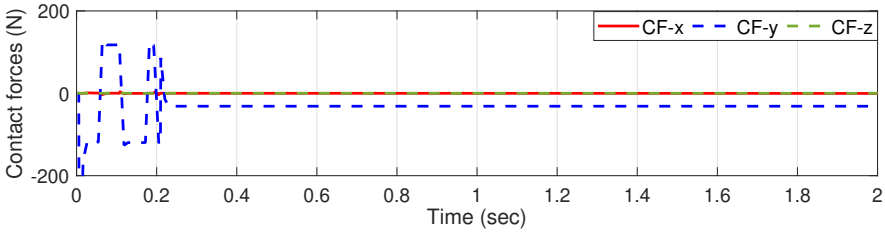

Fig. 15 Prismatic pair: Contact Forces against time.

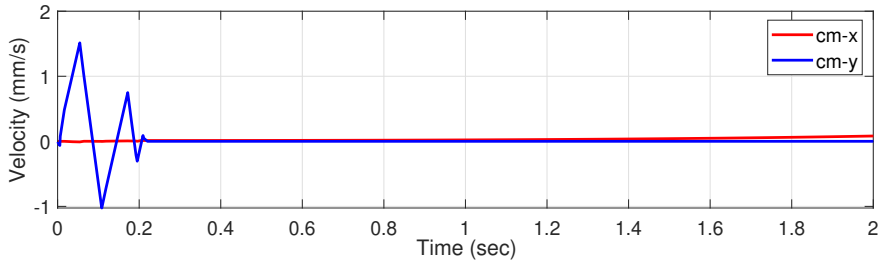

Fig. 16 Prismatic pair: X and Y velocities of center of mass.

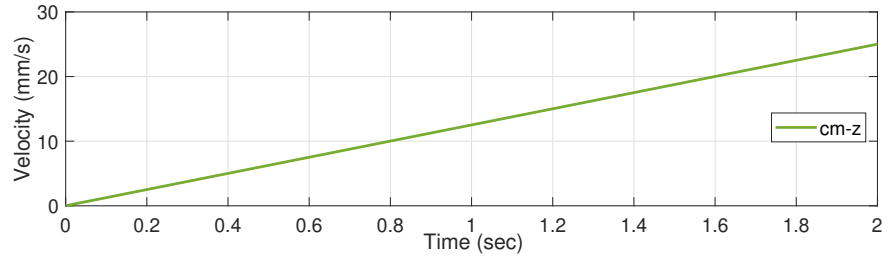

Fig. 17 Prismatic pair: Z velocity of center of mass.

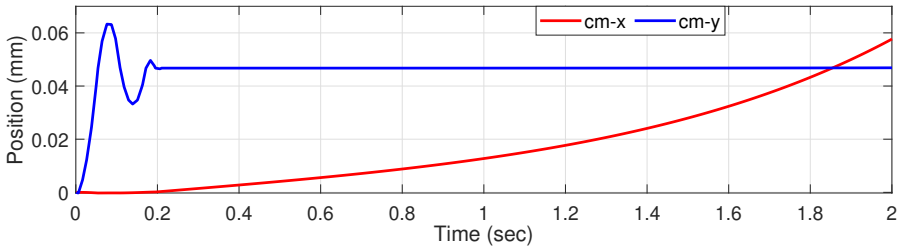

Fig. 18 Prismatic pair: X and Y positions of center of mass.

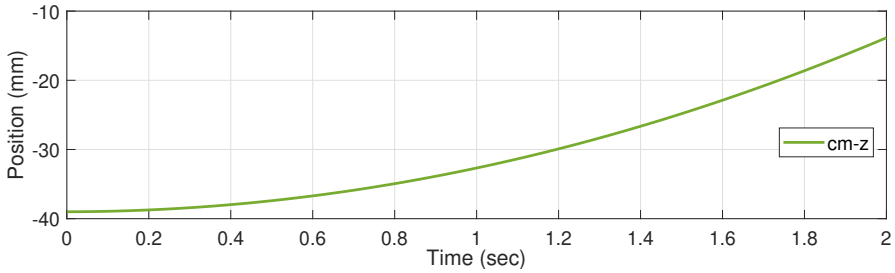

Fig. 19 Prismatic pair: Z position of center of mass.

using tangent space ODE formulation [20]. The rationale behind choosing a separate well-established methodology for simulating an ideal joint case was to check the credibility of the solution obtained from the method proposed in this work.

Figure 21 shows the positions of X and Y components of the contact points on the hinge pin's surface. It can be observed, that because of rotation, the system undergoes intermittent formation and breaking off of the contact. Figure 22 shows the contact forces $CF-x$, $CF-y$ and $CF-z$ in X, Y and Z directions respectively. The counterparts from an ideal joint case, i.e., without any clearance have also been compared. It can be observed that the general pattern of the variation of the contact forces is sinusoidal, excluding the peaks. When juxtaposed to the ideal-joint case, a similar pattern can be observed however, with a slight lag. This lag can be attributed to the fact that the pendulum, when released, first falls as a free body and consumes the clearance. Then the contact is made and the expected motion begins. Figure 23 represents the X

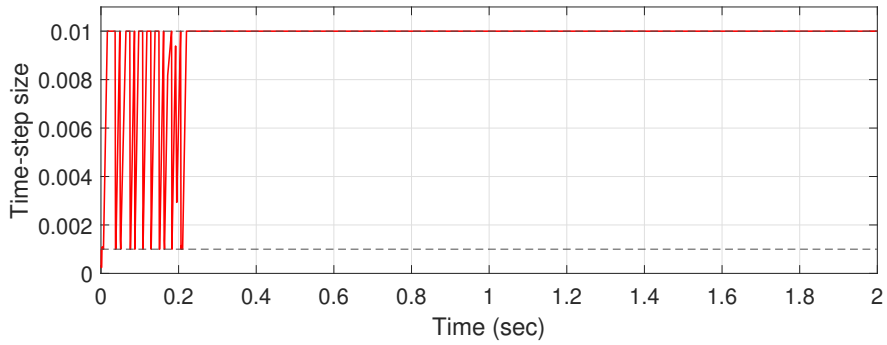

Fig. 20 Prismatic pair: Time step size.

and Y velocities of the center of mass and Figure 24 represents the Z-velocity of the center of mass.

The effect of lag can also be observed in the initial moments of time in Figure 23, while the rest of the velocity profiles overlap the ideal-joint counterparts. This overlap can also be observed in the position profiles. Figure 25 represent the positions of center of mass in X-Y plane. In Figure 26, The axial displacement of the center of mass of the pendulum is shown evolving with time. As can be expected, the ideal-joint case does not exhibit any displacement along Z direction. Furthermore, it must be noticed that the center of mass is located at a significant distance from the axis of rotation. Hence, the displacement of center of mass along Z is a combination of the tilting effect on the hinge pin because of radial clearance as well as the the prismatic displacement in Z direction because of axial clearance.

Figure 27 represents the variation of step-size with time. It can be observed that step-size changes when the contact points acquire high relative sliding speeds.

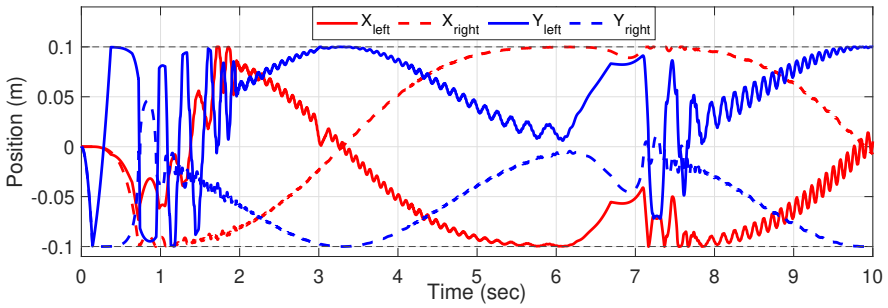

Fig. 21 Revolute pair: X and Y coordinates of the centers of left and right ends.

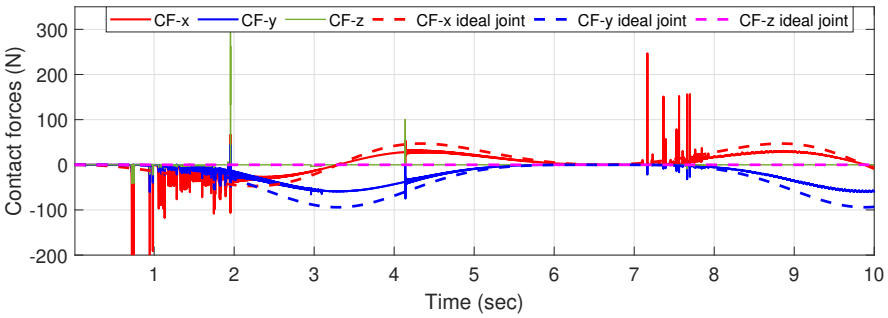

Fig. 22 Revolute pair with clearance and ideal revolute joint: Contact forces against time.

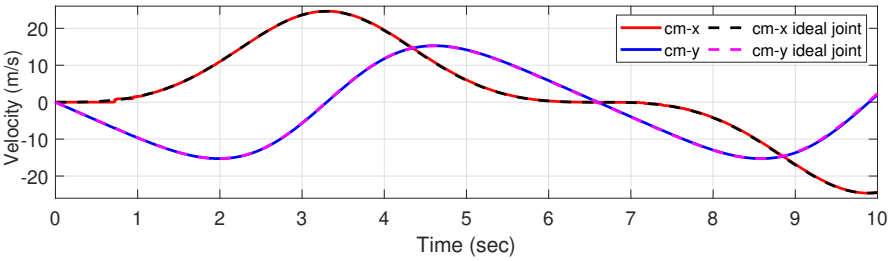

Fig. 23 Revolute pair with clearance and ideal revolute joint: X and Y velocities of center of mass.

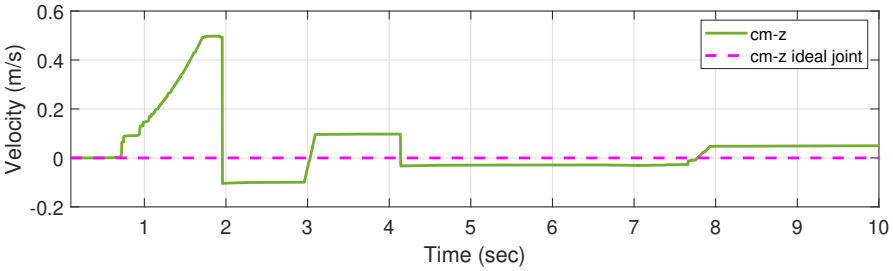

Fig. 24 Revolute pair with clearance and ideal revolute joint: Z velocity of center of mass.

6 Conclusions

The presented work complete formulations (for three most commonly used types of joints) for modeling and simulating multibody systems with clearances in the joints using non-smooth dynamics approach. The general NLP has been derived and special emphasis has been given on formulation of the constraint inequalities for the fundamental joints with clearances as functions of the geometry parameters of the bodies. The mathematical representations of constraint inequalities were carefully derived to ensure that they capture all the possible scenarios of contact formation. The simulation results demonstrate the efficiency of the non-smooth dynamics methodology for

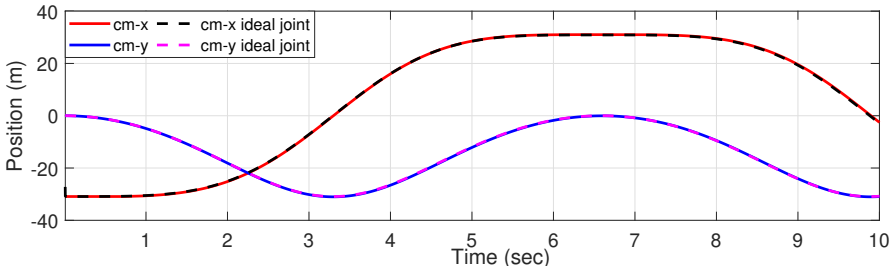

Fig. 25 Revolute pair with clearance and ideal revolute joint: X and Y coordinates of center of mass.

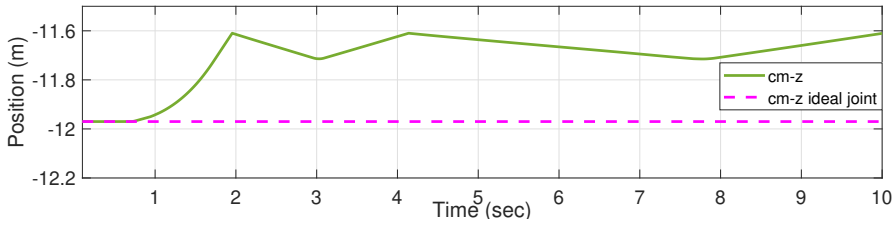

Fig. 26 Revolute pair with clearance and ideal revolute joint: Z coordinates of center of mass.

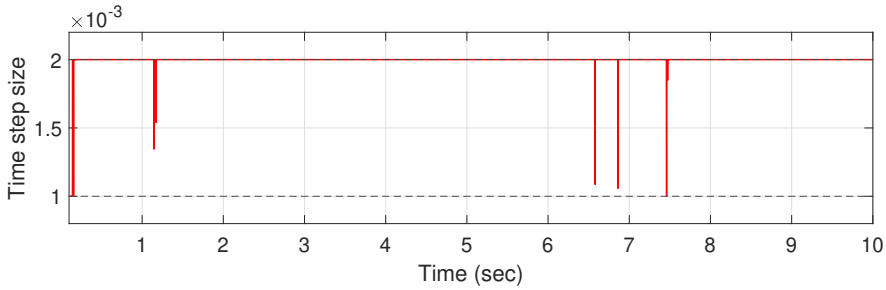

Fig. 27 Revolute pair with clearance: Time step size.

simulating the joints with clearance. The results showed that the tolerance limits of constraints during contact are also satisfied within significant accuracy.

The approach presented in this paper leverages on adaptive time step size adjustment by considering time step size h as a variable. Unlike traditional adaptive step-size integration algorithms where the error is controlled by using higher order methods, the formation or breaking-off of the contact is the only parameter being used in this work to control the step-size. Hence, there is further scope to formulate adaptive step-size control techniques for the presented non-smooth dynamics formulation. In addition to this, the definitions of the mechanical joints with clearances as parameters, as described in this document need to be further studied to examine if the same definitions can be used to simulate ideal joints with keeping the clearance $c = 0$. Its successful implementation would prove the versatility of the proposed formulation.

Though the scope of the presented work included frictionless contacts, an interesting inference may be drawn from the contact force plots. The magnitude of normal contact force varies significantly among the three cases discussed. Since the resisting friction force depends on the normal contact force's magnitude, adding friction to these simulations will impact the dynamic characteristics to a significant extent. Studying friction in clearance joints will further throw light upon the importance of clearances on the system's dynamics.

The industrial approach of assigning tolerances, and hence clearances, is primarily based on manufacturability related aspects. However, the effects of accumulated clearances on the kinematic and dynamic parameters of a mechanical system are often neglected. The presented work can be impactful in rationalizing the design procedures as tolerance assignment is a critical task on engineering drawings. Understanding the effect of tolerances on the system's dynamic response can be helpful in optimizing the design of a machine's components.

Acknowledgments. This work was supported by the Terramechanics, Multibody, and Vehicle Systems (TMVS) Laboratory and Computational Science Laboratory (CSL), Virginia Tech, Blacksburg, VA, USA.

Declarations

The authors declare that there are no conflicts of interests.

References

[1] Corral, E., Moreno, R., Meneses, J., Garcia, M., Castejón, C.: Spatial algorithms for geometric contact detection in multibody system dynamics. Mathematics 9 (2021) 1359 https://doi.org/10.3390/ math9121359.

[2] Dopico, D., Luaces, A., Saura, M., Cuadrado, J., Vilela1, D.: Simulating the anchor lifting maneuver of ships using contact detection techniques and continuous contact force models. Multibody System Dynamics 46 (2019) 147–179

[3] Dopico, D., Gonzalez, F., Cuadrado, J., Kövecses, J.: Determination of holonomic and non- holonomic constraint reactions in an index-3 augmented lagrangian formulation with velocity and acceleration projections. J. Comput. Nonlinear Dynam. 9 (2014) 041006

[4] Choi, J., Ryu, H., Kim, C., Choi, J.: An efficient and robust contact algorithm for a compliant contact force model between bodies of complex geometry. Multibody System Dynamics 23 (2010) 99

[5] Nikravesh, P., Lankarani, H.: A contact force model with hysteresis damping for impact analysis of multibody systems. Journal of Mechanical Design 112 (1990) 369–376.

[6] Shen, Y., Xiang, D., Wang, X., Wei, Y.: A contact force model considering constant external forces for impact analysis in multibody dynamics. Multibody System Dynamics 44 (2018) 397–419

[7] Sharf, I., Zhang, Y.: A contact force solution for non-colliding contact dynamics simulation. Multibody System Dynamics 16 (2006) 263–290

[8] Zakhariev, E.: Dynamics of rigid multibody systems with clearances in the joints. Mech. Struct. Mach. 27 (1999) 63–87

[9] Ibrahimi, S., Salahshoor, E., Nouri, S.: Sensitivity analysis for optimal design of multibody systems with clearance joint. Journal of Manufacturing Technology Management 11 (2018) 35–44

[10] Flores, P., Lankarani, H.: Dynamic response of multibody systems with multiple clearance joints. J. Comput. Nonlinear Dynam. 7 (2012) 031003

[11] Xiang, W., Yan, S., Wu, J., Niu, W.: Dynamic response and sensitivity analysis for mechanical systems with clearance joints and parameter uncertainties using chebyshev polynomials method. Mechanical Systems and Signal Processing 138 (2020) 106596

[12] Bauchau, O., Rodriguez, J., Bottasso, C: Modeling of unilateral contact conditions with application to aerospace systems involving backlash, freeplay and friction. Mechanics Research Communications 28 (2001) 571–599

[13] Jean, M.: The non-smooth contact dynamics method. Computer Methods in Applied Me- chanics and Engineering 177 (1999) 235–257

[14] Silcowitz-Hansen, M., Niebe, S., Erleben, K.: A nonsmooth nonlinear conjugate gradient method for interactive contact force problems. Vis. Comput. 26 (2010) 893–901

[15] Anitescu, M.: Optimization-based simulation of nonsmooth rigid multibody dynamics. Mathematical Programming 105(1) (2006) 113–143

[16] Negrut, D., Serban, R., Tasora, A.: Posing multibody dynamics with friction and contact as a differential complementarity problem. J. Comput. Nonlinear Dynam. 13 (2018) 014503

[17] Anitescu, M., Tasora, A.: An iterative approach for cone complementarity problems for nonsmooth dynamics. Comput. Optim. Appl. 47 (2010) 207–235

[18] Anitescu, M., Hart, G.D.: A constraint-stabilized time-stepping approach for rigid multibody dynamics with joints, contact and friction. Int. J. Numer. Methods Eng. 60(14), 2335–2371 (2004)

[19] Todorov, E.: Convex and analytically-invertible dynamics with contacts and constraints: Theory and implementation in mujoco. In: 2014 IEEE International Conference on Robotics and Automation (ICRA). (2014) 6054–6061 10.1109/ICRA.2014.6907751.

[20] Haug, E.J.: Computer-aided kinematics and dynamics of mechanical systems: basic methods. Allyn and Bacon Series in Engineering (1988)

[21] Gauß, C.: Über ein neues allgemeines grundgesetz der mechanik. Zenodo 13 (1829) 1448816 doi:10.1515/crll.1829.4.232.

[22] Anitescu, M., Tasora, A.: A Matrix-Free Cone Complementarity Approach for Solving Large-Scale, Nonsmooth, Rigid Body Dynamics. Comput. Methods Appl. Mech. Eng., 2011, 439–453.

[23] Xiao, Z.: A Comparative Analysis of an Interior-point Method and a Sequential Quadratic Programming Method for the Markowitz Portfolio Management Problem. Undergraduate thesis, Oberlin College, 2016.